ELSEVIER

Polymer 43 (2002) 2435–2444

polymer

www.elsevier.com/locate/polymer

Bidisperse melt polymer brush studied by self-consistent field model

Andreas F. Terzis*

Department of Physics, University of Patras, GR-26500 Patras, Greece

Received 16 July 2001; received in revised form 20 November 2001; accepted 7 December 2001

Abstract

We apply a lattice-based self-consistent mean-field (SCF) theory in order to investigate a dense bidisperse polymer brush. The system studied contains polyisoprene chains of 485 and 970 repeat units. We compare our results to neutron reflectivity experiments recorded at two different average surface densities of the grafted chains (0.323 and 0.455 nm^{-2}). We investigate the inner structure described by the bottom region, formed by a mixture of long and short chains, and the top region composed only of segments of the longer chains. The inner structure approximately scales with the total brush height, although small deviations occur. The width of the transition zone between the two regions seems to be independent of the brush height. The agreement between the experimental results and our SCF results is very good. We also systematically study the structure of the bidisperse brush for various values of the molar fraction of the longer chains, of the length ratios and of the overall surface densities.

Keywords: Bimodal molecular weight distribution; Dense polymer brush; Mean-field theory

1. Introduction

Polymer brushes are composed of polymer chains that are densely attached by one end to a solid usually non-interacting surface [1–6]. In polymer brushes the distance between grafted points is small compared to the macromolecular chain dimensions, hence strong overlap among neighboring chains is enforced. Consequently, the chains deform and stretch in the direction perpendicular to the interface. They are often formed by adsorption from solution, i.e. by bringing a solution containing end functionalized chains into contact with an interacting surface. The ends can either be chemically attached (quite high binding energy [7,8]) or physi-adsorbed (binding energy of the order of 10 k_BT [9–11]). The adsorbing, functional end could be a reactive group, or the immiscible block of a copolymer [12–16]. Applicability to colloidal stabilization, surface modification, adhesion, and lubrication has led to extensive experimental and theoretical study of these systems [4,5,17]. They also serve as testing ground for theoretical models due to their conceptual simplicity.

Initial theoretical and experimental studies of polymer brushes concentrated on monodisperse polymers. However, polydispersity, which is often an unavoidable feature of polymer systems (most commercial polymers has a broad molecular weight distribution), has been shown to affect the brush structure [18–23]. For example Milner et al. [19] applying a mean-field approximation, found that for a uniform distribution of chain lengths, the density profile changes completely. This was verified in the simulation reported in Ref. [21]. An understanding of the relationship between the molecular weight distribution and the brush properties is thus essential for purely scientific reasons and for engineering applications (i.e. tailoring the brush structure according to specific needs).

In this paper, we investigate a bidisperse melt polymer brush, i.e. a polymer brush in which the degree of penetration of the solvent into the brush is essentially negligible. We systematically investigate a bimodal molecular weight distribution as a model system for polydispersity. A bimodal brush consists of a mixture of shorter and longer chains and can be crudely divided into two regions: the bottom layer, which is adjacent to the surface and contains both short and long chain segments, and the top layer, which contains only segments of the longer chains. Many of our studies focused on the investigation of a bidisperse dense brush composed of an equimolar mixture of long and short chains, which differ in chain length by a factor of two. In addition, we study the dependence of the structure of the bidisperse brush on the tethering density. Finally, we systematically study the structure of the bottom and the top regions for various molar fraction of the longer chains and for various length ratios of the two chains.

* Tel./fax: +30-61-997-618.
E-mail address: terzis@physics.upatras.gr (A.F. Terzis).

0032-3861/02/$ - see front matter
PII: S0032-3861(01)00812-6

2. Theoretical backgrounds

A good starting point in order to describe the conformations and concentration profiles at polymer interfaces is the self-consistent mean-field (SCF) theory. The SCF theory was originally developed to treat bulk polymeric systems [24] and later developed by Dolan and Edwards [25,26] to treat polymers in inhomogeneous environments. Since then, the SCF theory has been applied to a variety of problems, including grafted polymer chains. The basic idea of this approach is to solve for the Green function of a random walk in the presence of the mean-field imposed by the repulsive and attractive interactions. This mean-field is a function of the density, which in turn is determined, self-consistently, by the average value obtained from the Green functions. The lattice version of the SCF theory was developed by Scheutjens and Fleer [27–29].

The self-consistent equations have an analytical solution for a particular limit, usually referred to as the classical limit [30]. The analytical theories [31–36] took advantage of the fact that in a system in which polymers are strongly stretched as in a brush, fluctuations around the most probable, or 'classical' paths are small and can be ignored to a first approximation. This theory was derived in the limit in which the thickness of the brush is infinitely greater than the unperturbed radius of gyration of the polymer composing it. In the analytical self-consistent field (aSCF) theories, the mutual interaction of the polymer chains is represented by a mean-field (referred to as 'kinematic' potential) that gives rise to a non-uniform stretching of the chains. The conformations of polymer chains are similar to the flight path of a particle starting at rest at the location of the free end and being accelerated in a field toward the 'bottom' of the brush. The field is a function of the position in the brush (i.e. distance from the surface). Chain length is proportional to the time of flight of the hypothetical particles. Stretching is equivalent to the velocity of the hypothetical particle. Kinematic potential has shown to be harmonic as the flight time is independent of the starting position [19]. aSCF theories have been extended in order to study dense polymer brushes following a bimodal molecular weight distribution [19,20]. For bimodal brush, the description has to accommodate two different flight times of the hypothetical particles. This can only be achieved if the ends of the shorter and the longer chains segregate into separate regions [19].

3. The numerical self-consistent field model

The self-consistent mean-field lattice model (SCF) developed by Scheutjens and Fleer has been used to describe polymer melts [37] and polymeric solutions near a solid substrate, polymers chemically attached to the substrate, rings, branched chains, copolymers, multi-component polymeric systems, and curved interfaces [6]. In order to develop a theoretical framework capable of describing realistic situations, the initial version of the SCF theory has been extended to incorporate conformational stiffness [38–40].

In our recent work [40], we have extended the Scheutjens and Fleer self-consistent field model for a system of macromolecular chains located close to a substrate. Some of the chains are terminally attached to the substrate (grafted chains). On the substrate it is also possible to find adsorbed (not chemically attached) segments. In Ref. [40], we have reformulated the SCF model in order to describe the most general case of free and terminally attached chains with various molecular weight distributions.

A three-dimensional (xyz) lattice of simple symmetry is assumed. The substrate is placed parallel to the xy plane; the resulting lattice layers of the polymer (planes parallel to the surface) are numbered consecutively, starting from the layer next to the surface ($z = 1$) and ending at a layer ($z = M$) where the presence of the substrate has negligible effect. Each layer is one lattice site thick and contains L lattice sites. Each lattice site has Z neighboring sites, a fraction λ_0 of which lie in the same layer and a fraction λ_1 of which lie in each of the adjacent layers. Z, the coordination number, reflects the point symmetries characterizing the lattice ($Z = 6$ for cubic and $Z = 12$ for hexagonal; $\lambda_0 = 2/3$ and $\lambda_1 = 1/6$ in both lattices). In order to describe a constant volume system, each lattice site has to be occupied by exactly one segment. A polymer molecule is represented by a chain of r^i connected segments, numbered $s = 1, 2, \ldots, r^i$. The index i is adopted to denote the type of the molecule. An additional index j is used in order to account for the polydispersity. Thus, chains appear with several sizes, r^i_j, where j varies from minimum to a maximum value. Moreover, from two consecutive segments we define the bond (b). In a cubic lattice the z-projection of a bond, reduced by the lattice constant, has three values. For two consecutive segments lying in layers z and $z + 1$, b is $+1$. For two consecutive segments lying in layers z and $z - 1$, b is -1. The value of b is 0 if both consecutive segments are lying in layer z. In other words, $b(\text{of segment } s) \equiv b_s = z_s - z_{s-1}$.

Each chain can assume a large number of possible conformations in the lattice. Each conformation (c) is defined by specifying the layer numbers in which each of the successive chain segments s finds itself (i.e. $c \equiv \{(s = 1, z = z_1), (s = 2, z = z_2), \ldots (s = r^i_j, z = z_{r^i_j})\}$). The number of chains (i, j) in conformation c is indicated as $n^c_{(i,j)}$. The chains are distributed over the various possible configurations (sets of conformations $\{n^c_{(i,j)}\}$) in the lattice with statistical weights depending on the energy and entropy of each configuration. The proper description of the system will be given in the context of statistical physics by means of the grand canonical partition function. The partition function is a sum of terms, each related to a specific configuration of the chains that fills the lattice. The non-bonded chain interactions are approximated using the Bragg–Williams mean-field approximation and the intrachain interactions are approximated using bending energies. The counting of

the number of ways of arranging chains over available sites is readily performed in a lattice model. Equilibrium is the state at which the chains are distributed over the various possible conformations in the lattice such that the free energy (derived from the partition function) is at its minimum. We make the assumption of replacing the sum of several terms in the partition function by its maximum term (i.e. zero fluctuations of the density in the (x, y) directions). In order to obtain an expression for the number of molecules $n^c_{(i,j)}$ of chain type i of size r^i_j in conformation c, we minimize the natural logarithm of the maximum term of the partition function with respect to $n^c_{(i,j)}$, subject to the full occupancy constraint applied layerwise. The system can be described in a mean-field self-consistent approximation in terms of a segment potential $u(z)$ depending only on the chemical nature of the segment, or, equivalently, in terms of a segment weighting factor ($G(z) = \mathrm{e}^{-u(z)/kT}$). The weight $G(z)$ is proportional to the probability of finding a segment in layer z of the interfacial system, relative to finding it in the bulk. Then the statistical weight for finding an end of an s-segment long chain in layer z, $G(z; s)$, is defined. It follows a recursion relation, which is solved once we know a proper initial condition. Then it is straight-forwarded to find the concentration of the end and non-terminal segments. Finally, by means of a composition law we find the volume fractions. The details of the SCF formalism are given in Refs. [27–29,37].

This simple SCF scheme has been extended in order to account for conformational stiffness [38–40]. Chain stiffness is introduced by assigning different bending energies to different bending angles formed by triplets of segments (or pairs of bonds). For a cubic lattice only 0° (back-folding or V conformer), 90° (L conformer) and 180° (straight or I conformer) bending angles are possible (see fig. 2 in Ref. [40]). The bending energies can be determined from the characteristic ratios [39,40]. To each bending energy (ε_b) we associate the corresponding Boltzmann factor $\tau_b = \exp(-\varepsilon_b/k_B T)$.

In a recent publication [40], we have extended SCF theory in order to treat more complex systems (i.e. polydisperse end-grafted chains). From now on, this modified version of the plain SCF theory, which treats both features (polydispersity and end-grafted chains) simultaneously, will be referred to as numerical self-consistent field (nSCF) theory. Actually, all equations derived in Ref. [40] are valid. But in melt polymer brush, we impose the constraint that the lattice is fully occupied exclusively by grafted chains. Hence, the number of layers, M is given by: $M = \bar{r}^g \tilde{\sigma}$, where $\bar{r}^g$ are the number-average molecular weight of the grafted chains and $\tilde{\sigma}$ the surface density of the grafted chains (i.e. percentage of the surface that is occupied by grafted chains).

4. Mapping real polymers onto the lattice

Among the possible choices for the lattice segment size, the ones that have been used the most are Kuhn and Flory segments. Equating the mean square end-to-end distance of a Kuhn chain represented by n_K Kuhn segments, each of length l_K, to the mean-square end-to-end distance of the real chain of n_b bonds, each of length l_b, with characteristic ratio C_∞, one has

$$\langle R^2 \rangle = C_\infty n_b l_b^2 = n_K l_K^2. \tag{1}$$

Equating the maximally extended length of a Kuhn chain to the maximally extended length of a real chain, with θ_b the angle between successive chemical bonds,

$$n_K l_K = n_b l_b \sin\left(\frac{\theta_b}{2}\right) \tag{2}$$

By combining these two expressions we find an expression for the Kuhn segment l_K,

$$l_K = l_b \frac{C_\infty}{\sin\left(\frac{\theta_b}{2}\right)}. \tag{3}$$

The Flory segment, of length l_F, is usually shorter; it corresponds to the length scale at which mixing occurs. A Flory segment can be defined such that a chain will have the same maximally extended length (end-to-end distance in all-*trans* conformation) and volume in the Flory segment representation as are measured experimentally [39,40].

Equating the volume of the Flory chain, containing r Flory segments, to the volume of a real chain

$$r l_F^3 = \frac{n_m M_m}{N_A \rho} \tag{4}$$

where n_m is the degree of polymerization, M_m the monomer molecular weight, ρ the mass density of the polymer and N_A is Avogadro's number.

Moreover, equating the length of the fully extended Flory chain to the maximally extended length of the real chain

$$r l_F = n_b l_b \sin\left(\frac{\theta_b}{2}\right) \tag{5}$$

where n_b is the number of chemical bonds per chain, l_b is the bond length and θ_b is the bond angle along the chain backbone.

By combining these equations, an expression for the length of the Flory segment is obtained,

$$l_F = \left[\frac{n_m M_m}{N_A \rho n_b l_b \sin\left(\frac{\theta_b}{2}\right)}\right]^{1/2}. \tag{6}$$

The bending energies are determined from the characteristic ratios by matching the mean-square end-to-end distance between a real chain and a chain of correlated Flory segments,

$$\langle R^2 \rangle = C_\infty n_b l_b^2 = C_\infty^F (r-1) l_F^2 \tag{7}$$

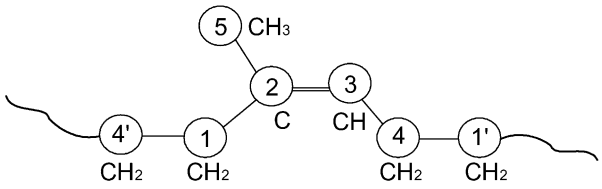

Fig. 1. United atom model for *cis*-1,4 polyisoprene. The atom numbering shown is used to describe bond angle and bond length values as given in Table 1.

in which C_∞^F is the characteristic ratio of the correlated Flory chain.

Assuming that $\tau_V = 0$ (i.e. back-folding is forbidden), the characteristic ratio of the Flory chain is related to the bending statistical weights by:

$$C_\infty^F = 1 + \frac{\tau_I}{2\tau_L} = 1 + \frac{1}{2}e^{(\varepsilon_L - \varepsilon_I)/kT}. \quad (8)$$

Since the characteristic ratio depends only on the difference between the energies ($\varepsilon_L - \varepsilon_I$), one (in our case ε_I) case may be set arbitrarily to zero. So the bending energy ε_L can be estimated once the characteristic ratio C_∞ is known.

Most researchers use the Kuhn segment as the unit segment. In our nSCF methodology, we use the Flory segments, in order to have correct representation of both polymer density and polymer stiffness.

5. Results and discussion

5.1. System studied

We apply our nSCF theory in order to investigate bidisperse dense brush (i.e. a brush in which the solvent is air and hence the degree of penetration of the solvent is negligible) composed of an equimolar mixture of short and long chains, which differ in chain length by a factor of two [41]. The chain lengths of the shorter and longer polyisoprene (PI) chains are approximately 485 and 970 repeat units (monomers), respectively. Polyisoprene is a very well studied polymer. Its united atom representation is shown in Fig. 1. Since the double bond constrains all five atoms in the *cis*-1,4 PI monomer to lie on the same plane, it is rather straightforward to map the *cis*-1,4 PI monomer onto an equivalent 'polymethylene' trimer. Hence, we represent PI monomer by an equivalent structure (see Fig. 2) that contains only single bonds. Simple geometrical considerations give that the length of the equivalent bond l_b is 3.1793 Å and the angle between two consecutive single bonds θ_b is 92.74° (Fig. 2). In the results produced by means of our nSCF method, we have assumed that the temperature of our system is 220 °C, which is the temperature at which experimental data [41] were collected. We use a mass density of 0.91 g cm^{-3}, a value derived from expressions, of the mass density as a function of the pressure and temperature, found in Ref. [42]. The value used in the present work for the characteristic ratio, C_∞, of the equivalent trimer was estimated to be 2.16 [42,43]. For this C_∞, Eqs. (6)–(8) give a bending energy $\varepsilon_L = 0.402k_BT$ ($\tau_L = 0.669$).

Table 1
Geometric parameters of *cis*-1,4 polyisoprene (see Fig. 1)

	Bond length (Å)
4′–1	1.53
1–2	1.51
2–5	1.51
2–3	1.34
3–4	1.51
	Bond angle (°)
$1\hat{2}3$	125
$2\hat{3}4$	125
$1\hat{2}5$	109
$2\hat{1}4'$	112
$3\hat{4}1'$	112

As in the experimental study, a mixture of h-PI and d-PI was used, the Flory segment used in out nSCF approximation, was the arithmetic mean value ($l_F = l_F$(h-PI) + l_F(d-PI))/2. From Eq. (6), we find $l_F = 5.3405$ Å, therefore the number of chemical (isoprene) monomers in a Flory segment is 1.1604. From Eq. (3), we found that the Kuhn statistical segment has a size almost twice the size of the Flory segment ($l_K = 9.4877$ Å).

The bidisperse brush is composed of longer a-chains with chain length r_a and shorter b-chains with chain length r_b Flory segments. The length ratio of the two chains is represented by $\varepsilon \equiv r_b/r_a$. The longer chains contain $r_a = 836$ Flory segments. The shorter chains contain $r_b = 418$ Flory segments. The total number of chains, n, per surface area, A, is given by $\sigma = n/A$, the number per unit surface of longer (shorter) chains is given by $\sigma_a(\sigma_b)$. Then, the molar fraction of the longer (shorter) chains is defined by $x_a(x_b) = \sigma_a(\sigma_b)/\sigma$. The polymer is regarded as incompressible. Hence the total height, H (in nm), of the bidisperse brush is given by the number-average chain length, $\bar{r}^g(= x_a r_a + (1 - x_a)r_b)$, and the number of chains per unit surface (overall surface density, σ): $H = l_F^3 \sigma \bar{r}^g$, where l_F is given in nm and surface density is expressed in nm^{-2}.

5.2. Comparison to experimental studies

The polymer brushes used in Ref. [41] were prepared by spreading mixtures of short and long polyisoprenes with

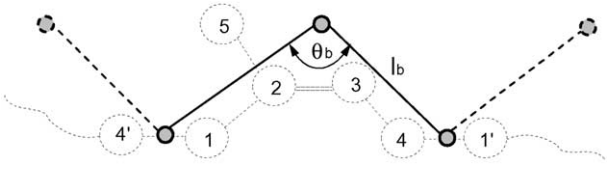

Fig. 2. Geometrical mapping of a *cis*-1,4 PI monomer onto an equivalent three-bead 'polymethylene' monomer.

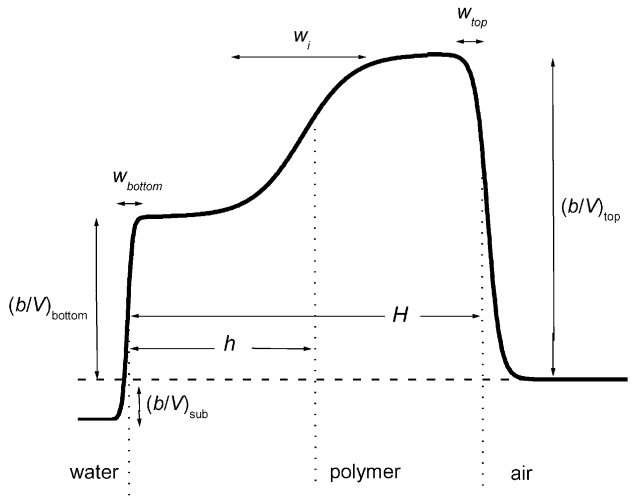

Fig. 3. Schematic drawing of the 'two-box' model of the scattering length density used for the simulation of the experimental neutron reflectivity profiles [41]. Our nSCF model is applied on the polymer region of thickness H.

quaternary ammonium headgroups onto the surface of a Langmuir trough filled with water. The neutron reflectivity profiles recorded at two different values of the mean areas per polymer chain, 220 and 310 Å^2, which corresponds to surface density of $\sigma = 0.455$ and 0.323 nm^{-2}. Authors of Ref. [41] analyzed their reflectivity profiles considering a 'two-box' model. This model is described by four scattering length densities (subphase, $(b/V)_{sub}$; bottom, $(b/V)_{bottom}$; top region of the brush, $(b/V)_{top}$; and air $(b/V)_{air} = 0$), three interfacial widths (bottom, w_{bottom}; inner, w_i; and top interface, w_{top}) and two lengths (height of bottom region, h, and total brush height, H) (outlined in Fig. 3). According to Ref. [41] the closest region to the solid surface (water phase, $w_{bottom} \sim 3.5$ Å $\sim l_F/2$) and the very top region (polymer/air, $w_{top} \sim 5$ Å $\sim l_F$), are very narrow. Therefore in our nSCF calculations we ignore these regions and we concentrate our study exclusively on the inner structure. Once we know $(b/V)_{bottom}$ and $(b/V)_{top}$ and by means of the volume fraction profiles obtained by our nSCF method we estimate the scattering length densities of the shorter chains (h-PI), $(b/V)_{h\text{-}PI}$, and the scattering length densities of the longer chains (d-PI), $(b/V)_{d\text{-}PI}$. Actually, the values used in our calculations in order to estimate the scattering length densities, are the ones reported in Table 2 in Ref. [41] (i.e. $(b/V)_{bottom} = 3.51 \times 10^{-6}$ Å^2 and $(b/V)_{top} = 6.94 \times 10^{-6}$ Å^2 for experiment with surface density $\sigma = 0.323$ nm^{-2} and $(b/V)_{bottom} = 3.58 \times 10^{-6}$ Å^2 and $(b/V)_{top} = 6.94 \times 10^{-6}$ Å^2 for experiment with surface density $\sigma = 0.455$ nm^{-2}).

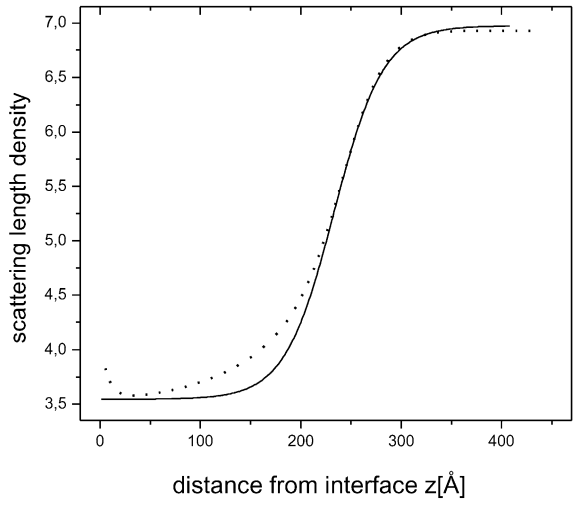

Fig. 4. Scattering length density profiles of monolayers of an equimolar mixture of d-PI and h-PI grafted at a solid surface, recorded at mean area per polymer chain at 220 Å^2 (solid line), compared with profiles predicted by nSCF model (dotted line). Units of scattering length density are 10^6 Å^{-2}.

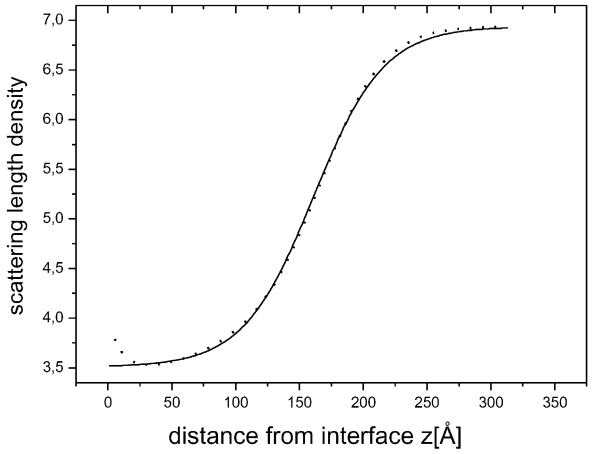

Fig. 5. Scattering length density profiles of monolayers of an equimolar mixture of d-PI and h-PI grafted at a solid surface, recorded at mean area per polymer chain at 310 Å^2 (solid line), compared with profiles predicted by nSCF model (dotted line). Units of scattering length density are 10^6 Å^{-2}.

In Figs. 4 and 5, we show the scattering length density profiles of an equimolar mixture of d-PI grafted chains and h-PI grafted chains recorded at surface densities mentioned before, and compare to profiles predicted by nSCF model. For both cases, the corresponding scattering length density profiles predicted by our nSCF method (dashed lines in both Figs. 4 and 5) are in good agreement with the experimental results (solid lines). More explicitly, the agreement is excellent for the lower surface density case ($\sigma = 0.323$ nm^{-2}, Fig. 5) and the agreement is very good for the higher surface density case ($\sigma = 0.455$ nm^{-2}, Fig. 4). We should point out that authors of Ref. [41] compared the corresponding scattering length density profiles to the profiles estimated by aSCF theories [19,20] and found very poor agreement (see figs. 6 and 7 in Ref. [41]).

5.3. Structural study of bidisperse brushes

Since our nSCF model reproduces experimental findings for dense bidisperse brush reasonably well, we pursue an nSCF-based systematic study of the dense bidisperse brush,

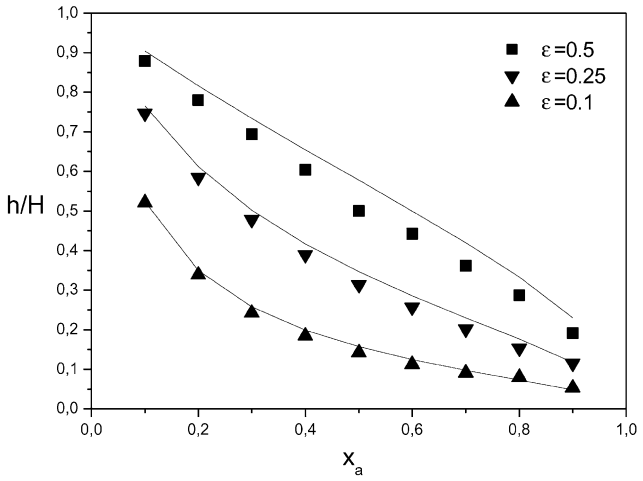

Fig. 6. Plots of the ratio of the height of the mixed region to the total brush height (h/H) as a function of the molar fraction of the longer chains, x_a, for various length ratios (ε) of the two chains. Data points correspond to $\varepsilon = 0.5$ (squares), $\varepsilon = 0.25$ (lower triangles) and $\varepsilon = 0.1$ (upper triangles). Solid lines depict the predictions of the aSCF theory.

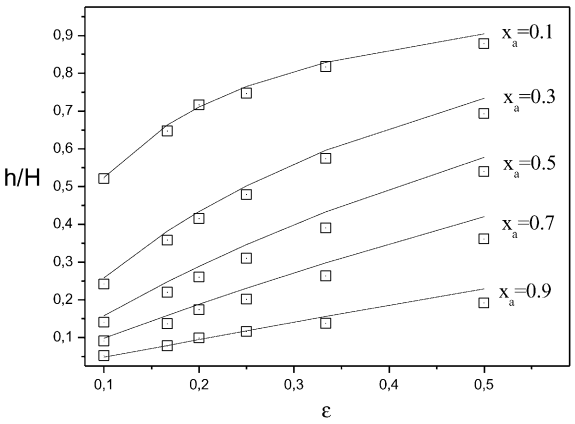

Fig. 7. Plots of the h/H ratio as a function of the length ratios (ε) of the two chains, for various molar fraction of the longer chains, x_a. From upper to lower set of data points, $x_a = 0.1$, 0.3, 0.5, 0.7 and 0.9. Solid lines describe the predictions of the aSCF theory.

a model system for studying the dense polydisperse brush. In Fig. 6, we plot the h/H ratio as a function of the molar fraction of the longer chains, x_a, for various length ratios of the long and short chains, ε ($= 0.1$, 0.25, 0.5), assuming fixed overall surface density of grafted chains ($\sigma = 0.5\ \mathrm{nm}^{-2}$). In our nSCF approximation, h is defined as the distance from the solid surface at which the long and short chains achieve equal volume fractions (i.e. h is an estimate of the height of the shorter chains). In the aSCF theories h is defined as the distance from the solid surface above which exclusively long chains are present. We observe that the aSCF results (solid line in Fig. 6) and the nSCF results (squares in Fig. 6) show very similar behavior. The largest difference is observed for length ratio of the two chains of one-half ($\varepsilon = 0.5$), which corresponds to the length ratio of the two chains used in the experimental study [41]. Our nSCF approximation predicts a simple functional form for the relationship between h/H and x_a, $h/H = \sqrt{(1 - x_a)/(1 + 1.6x_a)}$, which should be compared to $h/H = \sqrt{(1 - x_a)/(1 + x_a)}$ predicted by aSCF theories [19,20,41]. Actually, in the region $0.1 \le x_a \le 0.9$, nSCF model predicts a linear dependence between the h/H ratio and the molar fraction of the shorter ($1 - x_a$) or longer chains (x_a), ($h/H \sim 0.95 - 0.84x_a$). In all cases shown in Fig. 6, we observe that the nSCF results are systematically lower than the one obtained from the aSCF theories. Moreover, as the length ratio of the two chains (ε) decreases, the relative extension of the shorter chains (h/H) reveals a linear region of smaller extent ($0.5 < x_a < 0.9$). The slope of the linear part decreases as ε decreases, in agreement to what is expected for purely space-filling (entropic) reasons. For $\varepsilon < 0.5$, two distinct regions are reported. One corresponding to low molar fractions ($x_a < 0.4$) where the h/H ratio is more sensitive to changes in the molar fraction (x_a) and one almost linear region corresponding to high molar fractions ($x_a \ge 0.5$) where the h/H ratio is less sensitive to changes in the molar fraction (x_a).

In Fig. 7, we depict the h/H ratio as a function of the length ratio of the two chains (ε), for various molar fractions of the longer chains (x_a). All theoretical (nSCF) calculations were performed at a fixed overall surface density of $\sigma = 0.5\ \mathrm{nm}^{-2}$. For most cases, the predictions of the nSCF model (squares in Fig. 7) and the predictions of the aSCF theory (solid line in Fig. 7) are in good agreement. The worst agreement is observed for large values of ε and for large values of x_a. Working with large values of molar fraction of the longer chains, x_a, both mean-field methods (aSCF and nSCF) predict an almost linear relationship between the relative extension, h/H, and the length ratio of the two chains, ε. It is very instructive to observe that bidisperse mixtures containing more short chains ($x_a < 0.4$) show two distinct regions. One corresponding to low length ratios ($\varepsilon < 0.25$) where the h/H ratio increases abruptly with ε, and one corresponding to high length ratios ($\varepsilon \ge 0.25$) where the h/H ratio increases less abruptly with ε. For low concentration of long chains, the molar fraction, $1 - x_a$, is an indicator of how many short chains surround one long chain. Obviously, assuming fixed molar fraction of long chains (i.e. number of short chains surrounding one long chain), the larger the size of the long chains compared to the size of the short chains, the more the short chains will be influenced. As the size of the long chains decreases (i.e. ε takes values close to unity) the number of segments of the long chains that protrude from the surrounding short chains decreases too and its influence on the brush structure is less.

In Fig. 8, we study the h/H ratio as a function of x_a for $\varepsilon = 0.5$, considering various overall surface density of the grafted chains ($\sigma = 0.2$, 0.3, 0.5 and 0.8 nm^{-2}). Both aSCF theory (solid line) and the uniformly extended chain model (dotted line) predict affine deformation, i.e. the h/H ratio is independent of the brush thickness H or it is independent of

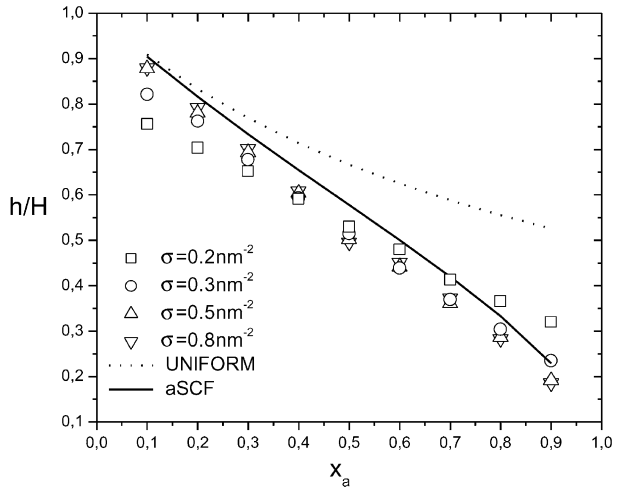

Fig. 8. Plots of the h/H ratio as a function of the molar fraction of the longer chains, x_a, for length ratio $\varepsilon = 0.5$ and for various overall surface densities. Points correspond to $\sigma = 0.2$ nm^{-2} (squares), $\sigma = 0.3$ nm^{-2} (circles) $\sigma = 0.5$ nm^{-2} (upper triangles) and $\sigma = 0.8$ nm^{-2} (lower triangles). Solid line describes the predictions of the aSCF theory (described in Refs. [19,20]). Dotted line describes the predictions of a simple analytical theory in which we assume that the chains are uniformly extended.

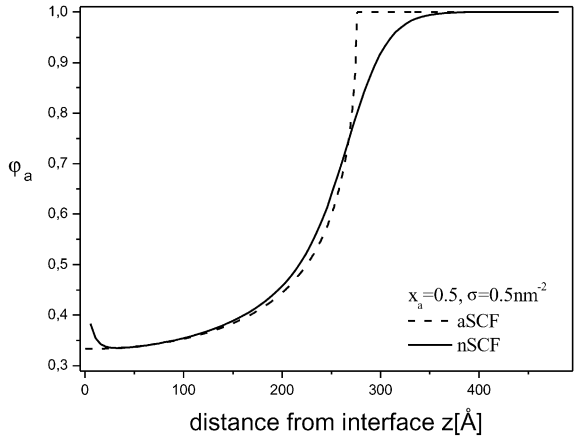

Fig. 9. Volume fraction profiles of longer chains, φ_a, for $\varepsilon = 0.5$, $x_a = 0.5$ and overall surface density of $\sigma = 0.5$ nm^{-2}. The solid line describes the prediction of our nSCF model and the dashed line the aSCF theory.

the surface density σ. But experiments [41] suggest that the h/H ratio seems to decrease slightly with increasing film thickness. In Fig. 8, we see that our nSCF model shows behavior in agreement with the experimental results. Specifically, our nSCF model predicts different behavior, depending on the relative amount of short and long chains. For low values of molar fraction of the long chains, x_a, as we increase the overall surface density the h/H ratio increases too. On the contrary, the behavior suggested by experiments on equimolar mixtures [41] (i.e. for $x_a = 0.5$, h/H ratio decreases with increasing surface density) is predicted by nSCF model for $x_a \geq 0.5$. Actually, the effect is enhanced as x_a is increased. The different behavior, depending on the molar fraction of the longer chains can be explained by means of the following argument. As the overall surface density is increased both short and long chains come closer, but they influenced in a different way. For high moral fraction of short chains ($x_a \rightarrow 0$), the upper segments of long chains may, depending on the length ratio of the two chains, interact with other long chains. On the contrary, short chain can not show a similar behavior, for high moral fraction of long chains ($x_a \rightarrow 1$ or $x_b \rightarrow 0$). Finally, we observe that most data points are near the line connecting the edge points ($h/H = 0, x_a = 1$) and ($h/H = 1, x_a = 0$). This behavior can be ascribed to the fact that in the brush regime the film thickness is proportional to the chain size.

Though our nSCF description of the brush has similar scaling to the aSCF description, its detailed predictions are substantially different. Actually, this is the reason for our nSCF results showing very good agreement with the experimental data, but the aSCF results do not agree satisfactorily with experimental results. In Fig. 9, we plot the volume fraction profiles of the longer chains, φ_a, for a system containing equal number of short and long chains ($x_a = 0.5$) with length ratio between the long and short chains of two ($\varepsilon = 0.5$), assuming an overall surface density of $\sigma = 0.5$ nm^{-2}. We observe that our nSCF theory predicts that the size of top region (composed exclusively of segments of longer chains) is much smaller than the one predicted by the aSCF theory. Consequently, we observe that in the top region the content of the shorter chains is higher than that predicted by the aSCF theory. Thus, compared with the predictions of aSCF theory, our nSCF method reports that the shorter chains are more stretched. Moreover, we predict that the content of long chains in the bottom region (solid line in Fig. 9), where a mixture of long and short chains coexists, is higher than that predicted by the aSCF theory (dashed line in Fig. 9). This is in agreement with the conclusions drawn from the experimental studies in Ref. [41].

The volume fraction profiles obtained in the context of our nSCF model have in most cases (except for very high surface density of grafted chains) a hyperbolic tangent functional form in agreement to several experimental studies [6,17].

Then, the volume fraction profile of each chain type (φ_a for long chains and $\varphi_b = 1 - \varphi_a$ for short chains) can be characterized by an effective interfacial width, w_i, determined by a hyperbolic tangent fit

$$\varphi_a(z) = \frac{\varphi_a(z = H) + \varphi_a(z = 0)}{2} + \frac{\varphi_a(z = H) - \varphi_a(z = 0)}{2} \tanh\left(\frac{2(z - h)}{w_i}\right). \quad (9)$$

where H is the height of the bidisperse brush, h the maximum extension of the shorter chains (defined as the distance from the substrate at which the volume fraction of the shorter chains is equal to the volume fraction of the free chains), and w_i is the interfacial width parameter. As the volume fraction profiles predicted by the aSCF theories cannot be fitted by a hyperbolic tangent function, it is not

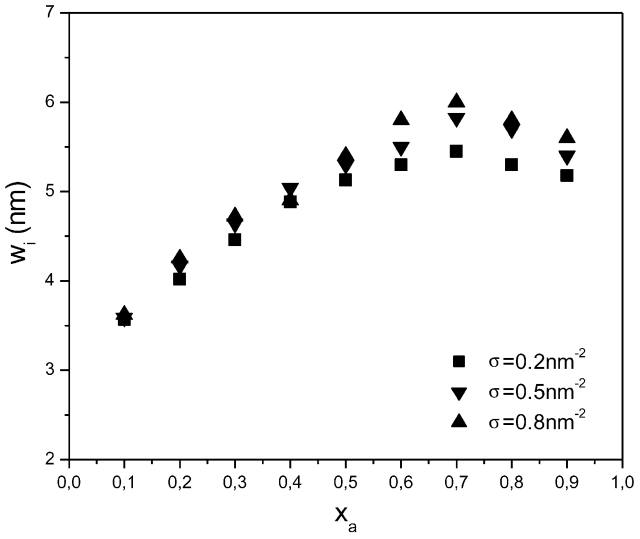

Fig. 10. Plots of the interfacial width, w_i, as a function of the molar fraction of longer chains, x_a, for given $\varepsilon = 0.5$ assuming various overall surface densities $\sigma = 0.2\ \mathrm{nm}^{-2}$ (squares), $\sigma = 0.5\ \mathrm{nm}^{-2}$ (lower triangles) and $\sigma = 0.8\ \mathrm{nm}^{-2}$ (upper triangles).

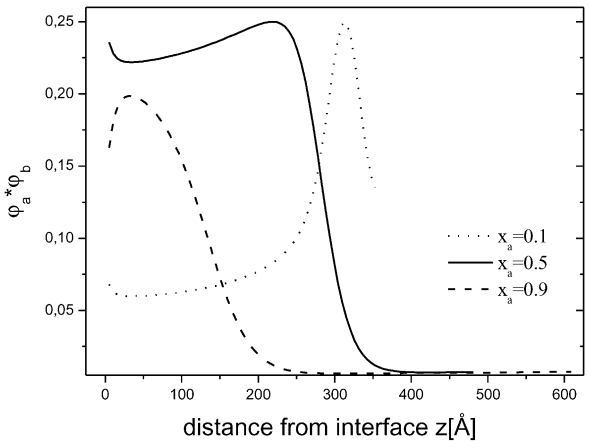

Fig. 12. Profiles of the product of the shorter and longer chain volume fractions, $\varphi_a\varphi_b \equiv \varphi_a(1-\varphi_a)$, for a bimodal brush with number-average chain length 418 Flory segments for the shorter chains and 836 Flory segments for the longer chains ($\varepsilon = 0.5$). Each curve corresponds to a different molar fraction of the longer chains. The molar fraction decreases from left to right. The values of x_a used in the calculations are 0.1, 0.5 and 0.9. In all cases the overall surface density is $0.5\ \mathrm{nm}^{-2}$.

straightforward to define an interfacial width. But as aSCF theories predict affine deformation, the thickness of the transition zone between the top and bottom regions, w_i, should change similarly. Experiments [41] do not agree with these predictions, as they have revealed that w_i seems to be unaffected by the change in brush thickness. Fig. 10 shows, that our nSCF results predict a behavior in agreement with experimental observations. Moreover, our study has shown that for $x_a < 0.6$ the interfacial width is unaffected by changes in brush thickness or equivalently by changes in the overall surface density of the grafted chains. For large values of molar fraction of long chains ($x_a \geq 0.6$) we report a slight dependence on the overall surface density. Finally, we report that for $x_a \sim 0.7$ the interfacial width reaches a maximum value.

In addition, we have systematically investigated the influence of the length ratio of long and short chains on the interfacial width of the mixed region. In Fig. 11, we observe that the interfacial width reaches a maximum value for all cases studied by nSCF method ($\varepsilon = 1/10$, 1/5 and 1/3). The value of the molar fraction of the longer chains, x_a, at which the maximum occurs, is shifted toward lower values as we decrease ε.

The behavior reported in Figs. 10 and 11 will be investigated further by studying the region where long and short chains coexist. In order to investigate this region, we study the product of the volume fractions ($\varphi_a\varphi_b \equiv \varphi_a(1-\varphi_a)$), which takes non-zero values when volume fractions of both short and long chains have appreciable value. In Fig. 12, we plot the $\varphi_a\varphi_b$ products as a function of the distance from the substrate for three different molar fractions of the long chains. In all cases studies we assume an overall surface density of $0.5\ \mathrm{nm}^{-2}$ and $\varepsilon = 0.5$. For $x_a = 0.1$, where we have very few long chains the thickness of the brush is mainly determined by the size of the shorter chains (we should recall that in the brush regime, thickness is proportional to the contour length of the polymeric chain), in accordance to what was predicted from the h/H ratio dependence (see Fig. 6), where we have reported a value of $h/H \sim 0.9$. In this case long and short chains coexist everywhere. But longer chains contain more segments (twice the number of segments of the shorter chains) than the shorter chains. Those segments of the longer chains are accommodated in the top region (Fig. 14(a)). Therefore, in this region we have comparable number of segments belonging to short chains (as molar fraction of shorter is high $1 - x_a = 0.9$) and to long chains (see Fig. 12, dotted line). In this case we

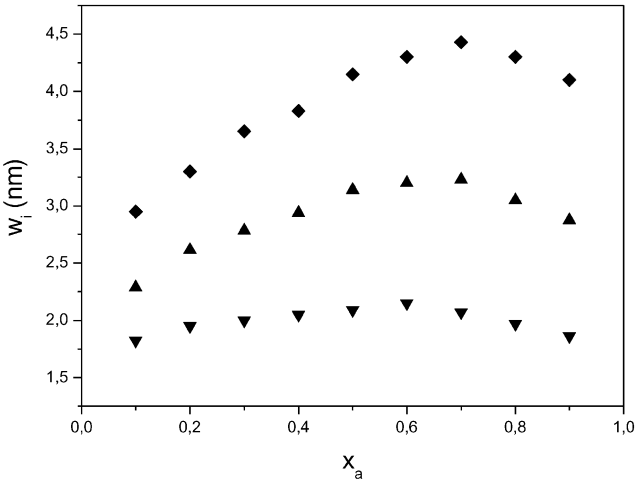

Fig. 11. Plots of the interfacial width, w_i, as a function of the molar fraction of longer chains, x_a. The overall surface density is $\sigma = 0.5\ \mathrm{nm}^{-2}$. The length ratio, ε, takes several values ($\varepsilon = 1/3$ represented by diamonds, $\varepsilon = 1/5$ represented by upper triangles, and $\varepsilon = 1/10$ represented by lower triangles).

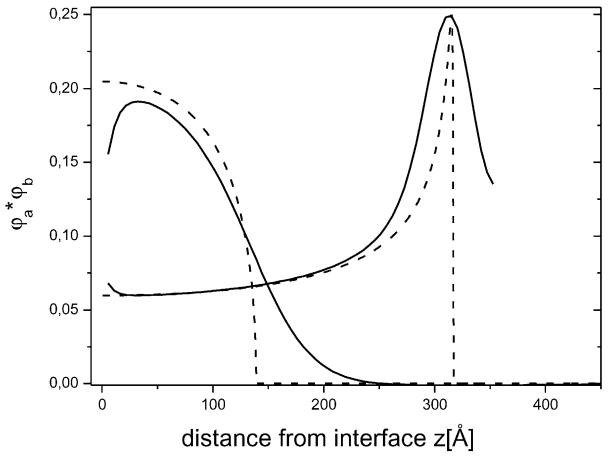

Fig. 13. Profiles of the product of the shorter and longer chain volume fractions, $\varphi_a\varphi_b \equiv \varphi_a(1-\varphi_a)$, for a bimodal brush with number-average chain length 418 Flory segments for the shorter chains and 836 Flory segments for the longer chains ($\varepsilon = 0.5$). The overall surface density is 0.5 nm^{-2}. Each curve corresponds to a different molar fraction of the longer chains. The molar fraction decreases from left to right. The values of x_a used in the calculations are 0.1 and 0.9. Solid lines represent the predictions of our nSCF method. For comparison we plot the predicted profiles from aSCF theories.

see that the shorter chains and the lower part of the longer chains are almost equally stretched, but obviously the upper segments of the longer chains are much less stretched as we assume that our dense brush is incompressible (see Fig. 14(a)).

We then discuss the case where we have equal number of short and long chains ($x_a = 1 - x_a = x_b = 0.5$). In that case for distances from the substrate up to h, both short and long chains coexist at equal amount (see Fig. 12, solid line). This is why we observe almost constant value for the product $\varphi_a\varphi_b$. But at the top region, $H - h$, which was predicted to be of the same size as h (as $h/H \sim 0.5$ from Fig. 6), purely long chains exist and the product $\varphi_a\varphi_b$ has small value. The structure of the equimolar bidisperse dense brush is shown in Fig. 14(b).

We finally investigate the case where our system contains a lot of long chains and consequently very few short chains. Here the region of coexistence between short and long chains is defined exclusively from the bottom region (see Fig. 12, dashed line). Again, this is in accordance to the picture envisioned from the h/H ratio study, where we reported a value of 0.20 (see Fig. 6).

In Fig. 13, we compare nSCF (solid lines) and aSCF (dotted lines) results. We see different behavior mainly for $z > h$ as it is expected (see Fig. 9). We can define an interfacial width w_{coex} as:

$$w_{coex} \equiv 4\int_0^\infty \mathrm{d}z\, \varphi_{long}\varphi_{short}. \tag{10}$$

It can be easily shown that $w_{coex} \propto w_i$, once the volume fraction profiles follow a hyperbolic tangent profile (Eq. (9)). The

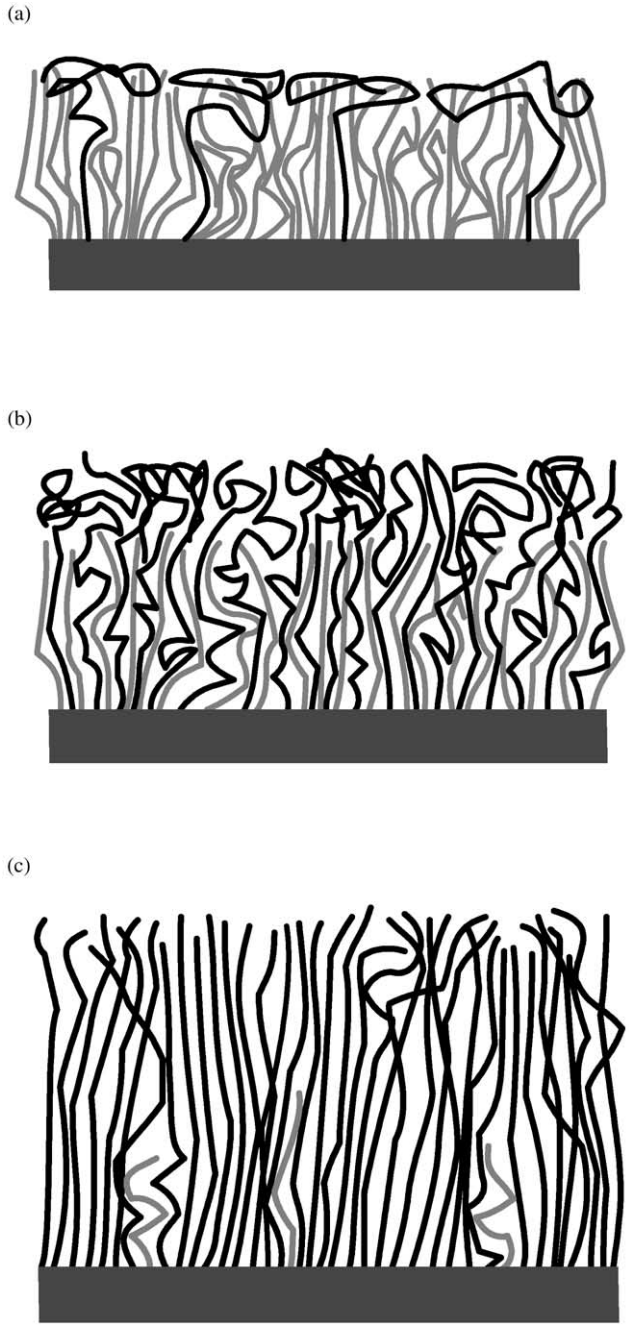

Fig. 14. Bimodal brushes. (a) Few long chains immersed in an environment of short chains ($x_a = 0.1$). The shorter chains determine the thickness of the brush. The top region of the brush is the region where shorter and longer chains intermingle more. (b) Bimodal brush containing equal number of shorter and longer chains ($x_a = 0.5$). There is a wide region, starting from the region very close to the solid surface, where shorter and longer chains coexist. (c) Few short chains immersed in an environment of long chains ($x_a = 0.9$). The longer chains determine the thickness of the brush. The bottom region of the brush is the region where shorter and longer chains coexist.

w_{coex} calculated by means of both mean-field methods (nSCF and aSCF) follows the behavior depicted in Fig. 10.

Obviously, a specific length ratio of long and short chains, ε, can be achieved by several combinations of r_a and r_b.

A preliminary study has not shown any system size effects on the h/H ratio. On the contrary, the interfacial width is a function of r_a and ε (i.e. $w_i = w_i(\varepsilon, r_a)$).

6. Conclusions

The dense bidisperse polymer brush is an inhomogeneous system. Close to the plane of tethering, short and long chains coexist. On the contrary, the top region of the brush composed of very few short chains. Depending on the overall surface density, the molar fraction of the longer chains and the length ratio between long and short chains, this region might contain purely long chains. The aSCF theories predict very abrupt vanishing of the volume fraction of the shorter chains. This behavior is not supported by the experimental studies [41] and our findings.

In the system studied here, our nSCF approach (i.e. extended SCF model, in order to describe polydisperse grafted polymer chains) gives results in very good agreement with the experimental results, practically without fitting parameters.

For a dense bidisperse polymer brush of $\varepsilon = 0.5$ and $x_a = 0.5$, our nSCF results show that the width of the transition zone between the mixed region and the top region is independent of the height of the brush, in agreement to experimental results [41]. Moreover, our studies for the same system, show a deviation from affine deformation (i.e. changes in the relative height of the mixed region upon changing the brush height) consistent with indication from the experimental work [41].

In conclusion, we suggest more experiments to clarify and check behavior predicted by nSCF models, as bidisperse brush is a prototype system for polydisperse systems (and in most practical cases we have polydisperse polymers). Our major predictions are (a) that the ratio of the height of the mixed region to the total brush height depends on the overall surface density in a way which is sensitive to the value of the molar fraction of the two chains and (b) that the interfacial width shows a maximum.

Finally, we would like to point out, that our method is quite general and can be applied for any polydisperse systems (for example, trimodal molecular weight distribution, uniform molecular weight distribution, Flory most probable molecular weight distribution etc.).

In conclusion, we say that in this work we have shown that our extended version of the SCF (nSCF) model is a very powerful computational tool for treating realistic polymeric systems. It is known that aSCF theories usually give qualitative agreement. On the contrary, our nSCF approach gives adequate quantitative agreement with experimental results. Recently, this approach was applied with great success in similar polymeric systems [44,45].

Acknowledgements

We would like to thank Prof. Doros N. Theodorou and Dr Costas Daoulas for many valuable discussions. Computational resources for this research were made available by the Educational and Initial Vocational Training Program on Polymer Science and Technology-3.2a. 33H6.

References

[1] Doran AK, Edwards SF. Proc R Soc 1975;A343:427.
[2] Alexander SJ. J Phys (Paris) 1976;38:977.
[3] DeGennes P-G. Macromolecules 1980;13:1069.
[4] Milner ST. Science 1991;252:905.
[5] Harpelin A, Tirrell M, Lodge TP. Adv Polym Sci 1992;100:31.
[6] Fleer GJ, Cohen Stuart MA, Scheutjens JM, Cosgrove T, Vincent B. Polymers at interfaces. Cambridge: Chapman & Hall, 1993.
[7] Auroy P, Auvray L, Leger L. J Phys Condens Matter 1990;2:317.
[8] Auroy P, Mir Y, Auvray L. Phys Rev Lett 1992;69:93.
[9] Taunton HJ, Toprakcioglu C, Fetters LJ, Klein J. Nature 1988;332:712.
[10] Taunton HJ, Toprakcioglu C, Fetters LJ, Klein J. Macromolecules 1990;23:571.
[11] Klein J, Perahia D, Warburg S. Nature 1991;352:143.
[12] Tirrell M, Patel S, Hadziioannou G. Proc Natl Acad Sci 1987; 84:4725.
[13] Ansarifar MA, Luckham PF. Polymer 1988;29:329.
[14] Taunton HJ, Toprakcioglu C, Klein J. Macromolecules 1988;21:3333.
[15] Cosgrove T, Heath T, van Lent B, Leermakers F, Scheutjens JM. Macromolecules 1988;20:1692.
[16] Patel SS, Tirrell M. Ann Rev Phys Chem 1989;40:597.
[17] Jones RAL, Richards RW. Polymers at surfaces and interfaces. Cambridge: Cambridge University Press, 1999.
[18] Tirrell M, Parsonage E, Watanabe H, Dhoot S. Polym J 1991;23:641.
[19] Milner ST, Witten TA, Cates M. Macromolecules 1989;22:853.
[20] Birshtein TM, Liatskaya YuV, Zhulina EB. Polymer 1990;31:2185.
[21] Chakrabarti A, Toral R. Macromolecules 1990;23:2016.
[22] Lai PY, Zhulina EB. Macromolecules 1992;25:5201.
[23] Dan N, Tirrell M. Macromolecules 1993;26:6467.
[24] Edwards SF. Proc Phys Soc (Lond) 1965;85:613.
[25] Doral AK, Edwards SF. Proc R Soc Lond 1974;A337:509.
[26] Doral AK, Edwards SF. Proc R Soc Lond 1975;A343:427.
[27] Scheutjens JM, Fleer GJ. J Phys Chem 1979;83:1619.
[28] Scheutjens JM, Fleer GJ. J Phys Chem 1980;84:178.
[29] Scheutjens JM, Fleer GJ. Macromolecules 1985;18:1882.
[30] Netz RR, Schick M. Macromolecules 1998;31:5105.
[31] Milner ST. Europhys Lett 1988;7:695.
[32] Milner ST, Wang ZG, Witten TA. Macromolecules 1989;22:489.
[33] Milner ST, Witten TA. Macromolecules 1992;25:5495.
[34] Zhulina EB, Borisov OV, Pryamitsyn VA, Birshtein T. Macromolecules 1991;24:140.
[35] Zhulina EB, Borisov OV, Brombacher L. Macromolecules 1991; 24:4679.
[36] Lyatskaya YV, Leermakers FAM, Fleer GJ, Zhulina EB, Birshtein TM. Macromolecules 1995;28:3562.
[37] Theodorou DN. Macromolecules 1988;21:1400.
[38] Wijmans CM, Leermakers FAM, Fleer GJ. J Chem Phys 1994;101:8214.
[39] Fischel LB, Theodorou DNJ. Chem Soc Faraday Trans 1995;91:2381.
[40] Terzis AF, Theodorou DN, Stroeks A. Macromolecules 2000;31: 1312.
[41] Goedel WA, Luap C, Oeser R, Lang P, Braun C, Steitz R. Macromolecules 1999;32:7599.
[42] Mark JE. Physical properties of polymers handbook. WoodBury, NY: American Institute of Physics Press, 1996.
[43] Mattice WL, Suter UW. Conformational theory of large molecules. New York: Wiley, 1994.
[44] Retsos H, Terzis AF, Anastasiadis SH. In press.
[45] Daoulas C, Terzis AF, Mavrantzas VG. Submitted for publication.